System Identification of Small-Size Unmanned Helicopter Dynamics

Bernard Mettler
Department of Mechanical Engineering
Carnegie Mellon University
Pittsburgh, Pennsylvania

Mark B. Tischler
Army/NASA Rotorcraft Division
Aeroflightdynamics Directorate (AVRDEC)
US Army Aviation and Missile Command
Ames Research Center

Takeo Kanade
The Robotics Institute
Carnegie Mellon University
Pittsburgh, Pennsylvania

***Abstract*: Flight testing of a fully-instrumented model-scale unmanned helicopter (Yamaha *R-50* with 10ft. diameter rotor) was conducted for the purpose of dynamic model identification. This paper describes the application of CIFER® system identification techniques, which have been developed for full size helicopters, to this aircraft. An accurate, high-bandwidth, linear state-space model was derived for the hover condition. The model structure includes the explicit representation of regressive rotor-flap dynamics, rigid-body fuselage dynamics, and the yaw damper. The R-50 configuration and identified dynamics are compared with those of a dynamically scaled UH-1H. The identified model shows excellent predictive capability and is well suited for flight control design and simulation applications.**

1 Introduction

The interest in unmanned aerial vehicle (UAV) systems with helicopter-like capabilities for both civil and military applications, is becoming well established. The US Navy, for example, is developing a vertical takeoff and landing tactical unmanned aerial vehicle (VTUAV) for a wide range of ship and land-based missions. Ship-based operations include automatic take-off and recovery in up to 25-40kts wind and ship deck motion of up to +/-8deg roll [1].

In order for helicopter-based UAVs (HUAVs) to be useful, it is crucial that the flight-control system does not restrict their attractive attributes: the extended flight-envelope and the capability for vertical take-off and landing. Today, progress in the development of HUAVs is mainly hindered by the complexity of the modeling and flight-control design and by the absence of efficient tools to support these tasks.

In general, the design of flight control systems for helicopters is a difficult problem. Unlike fixed-wing UAVs, the bare airframe HUAV exhibits a high degree of inter-axis coupling, highly unstable and non-minimum phase dynamic characteristics, large response variations with flight condition, and large delays associated with the rotor. The broad performance potential of the helicopter is in fact directly related to the complex character of its flight-dynamics, which are responsible for a number of difficult control issues. Maneuverability is related to fast or even unstable dynamics, and the strong control response is related to a high sensitivity to inputs (including disturbances such as wind gusts).

The complexity of helicopter flight dynamics makes modeling itself difficult, and without a good model of the flight-dynamics, the flight-control problem becomes inaccessible to most useful analysis and control design tools. The goal of achieving good control performance translates directly to accuracy and bandwidth requirements of the model [2]. High-bandwidth models are also important for simulation, improvement and validation of first-principle based models, and the evaluation of handling qualities. More generally, the ability to derive accurate dynamic models using real flight-data represents a key part in the integration of the flight-control design process.

System identification has been very successful in full-size helicopters. This efficient application of system identification to helicopters is due in large part to the high level of technicality involved in the procedure and the tools. These techniques, if applied properly, should be equally successful for small-size unmanned helicopters.

This paper presents a detailed example of the application of a full-size helicopter's identification methods to a small-size unmanned helicopter in hover flight. The goal of this experiment is to determine how well the full-size system identification techniques apply to small-size unmanned helicopters, and see whether accurate models can be derived through this procedure. The experiment also represents an opportunity to understand the dynamics of small-size

Presented at the American Helicopter Society 55th Forum, Montreal, Quebec, Canada, May 25-27, 1999.
Copyright © 1999 by the American Helicopter Society, Inc. All rights reserved.

helicopters in light of what is known about full-size helicopters. Dynamic scaling rules are used to compare the configuration and identified dynamics of the small-size R50 with the full-size UH-1H helicopter. This is especially interesting here because the comparison takes place within the specific framework of system identification, thereby allowing for simple and explicit analyses ranging from questions about the model structure to more precise aspects such as the modal characteristics or even physical parameters.

Figure 1a - Instrumented *R50* in hovering flight

2 Description of the Helicopter

The helicopter used for the identification experiment is a Yamaha *R-50* modified by Carnegie Mellon's Autonomous Helicopter project [3] for research in vision-based autonomous flight. The *R*-50 is a commercially available small-size helicopter originally designed for crop-dusting applications.

The *R-50* uses a two-bladed teetering main rotor with a Bell-Hiller stabilizer bar. The relatively rigid blades are connected to the hub via a yoke which offers independent flapping motion through elastomer fittings. The yoke is attached to the rotor shaft over the teetering hinge in an underslung configuration, eliminating the Coriolis forces and the associated in-plane blade motion. The teetering motion is also restrained by an elastomer damper/spring. This rotor system is stiffer than classical teetering rotors.

The Bell-Hiller stabilizer consists of a pair of paddles that mechanically provides a lagged rate (or "pseudo-attitude") feedback in the pitch and roll loops [4]. The low frequency dynamics are stabilized, which substantially increases the phase margin for pilot/vehicle system in the crossover frequency range (1-3 rad/sec) [4]. The pseudo-attitude feedback also reduces the response of the aircraft to wind gusts and turbulence. These improvements in aircraft handling and low-frequency stability are achieved at the expense of increasing the response time constant of the rotor to about 5 rotor revs, thereby reducing the damping in the coupled fuselage/rotor-flap dynamics. Additional characteristics of the *R-50* are given in Table 1 and Figure 1b. Figure 1a shows Carnegie Mellon's instrumented *R-50* in hover flight.

Helicopter Instrumentation

Carnegie Mellon's instrumented helicopter represents an excellent platform for the identification experiments because of its state-of-the-art instrumentation, which provides high quality flight-data.

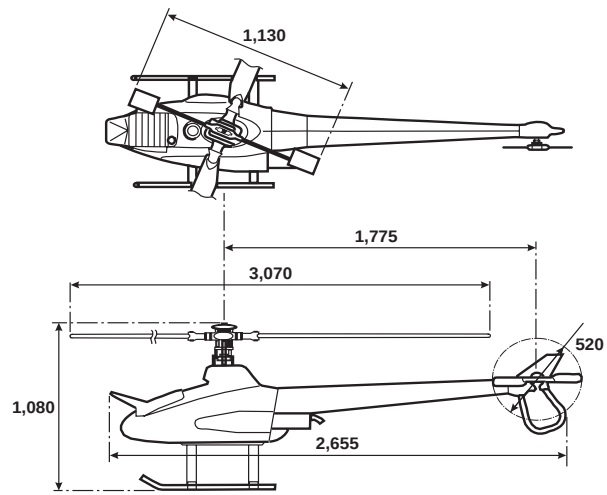

Figure 1b - *R50* dimensions (mm)
(based on *R50* Operating Manual)

Dimensions	see Figure 1a
Rotor speed Tip speed	850 rpm 449 ft/sec
Dry weight Instrumented (full payload capability)	97 lbs 150 lbs
Engine type	water cooled, 2-stroke, 1 cylinder
Flight autonomy	30 minutes

Table 1 – *R50* physical characteristics

The centerpiece of the helicopter onboard systems is a VME-based on-board flight computer which hosts a Motorola *68060* processor board and a sensor I/O board. All sensors and actuators of the helicopter connect through the I/O board with the exception of the inertial measurement unit (IMU), which connects directly to the processor board through a special serial port. The communication to the ground station takes place via wireless Ethernet. This system runs under a VxWorks real-time operating system.

Three linear servo-actuators are used to control the swash plate, while another controls the pitch of the tail rotor. The dynamics of all the actuators have been identified separately as first order. The engine speed is controlled by a governor which maintains the rotor speed constant in the face of changing rotor load.

Three navigation sensors are used: a fiber-optic based inertial measurement unit (IMU), which provides measurements of the airframe accelerations a_x, a_y, a_z, and angular rates p, q, r (resolution: 0.002 g and 0.0027^o, data rate: 400 Hz); a global positioning system (GPS) (precision: 2 cm, update rate: 4 Hz); and a magnetic compass for heading information (resolution: 0.5^o, update rate: 2 Hz).

The IMU is mounted on the side of the aircraft, and the GPS and compass are mounted on the tail. Each measurement is corrected for its respective offset from the center of gravity (c.g.). The c.g. location is known only approximately.

A 12th order Kalman filter running at 100 Hz is used to integrate the measurements from the IMU, GPS and compass to produce accurate estimates of helicopter position, velocity and attitude.

3 Frequency-domain Identification Techniques

Frequency responses fully describe the linear dynamics of a dynamical system. When the system has nonlinear dynamics (as all real physical systems do), system identification determines the describing functions which are the best linear fit of the system response based on a first harmonic approximation of the complete Fourier series. For the identification, the frequency domain method known as CIFER® (Comprehensive Identification from Frequency Responses) [5] was used. While CIFER® was developed by the U.S. Army and NASA specifically for rotorcraft applications, it has been successfully used in a wide range of fixed and rotary-wing, and unconventional aircraft applications [6]. CIFER® provides a set of utilities to support the different steps of the identification process. All the tools are integrated around a database system which conveniently organizes the large quantity of data generated throughout the identification.

The different steps involved in the identification process are:

Collection of flight-data. The flight-data is collected during special flight experiments.

Frequency response calculation. The frequency response for each input-output pair is computed using a Chirp-Z transform. At the same time, the coherence function for each frequency response is calculated.

Multivariable frequency domain analysis. The single-input single-output frequency responses are conditioned to remove the cross axis effects. The partial coherences are computed.

Window Combination. The accuracy of the low and high frequency ends of the frequency responses is improved through optimal combination of frequency responses generated using different window lenghts.

State-space identification. The parameters (derivatives) of an a priori-defined state-space model are identified by solving an optimization problem driven by frequency response matching.

Time Domain Verification. Finally, to evaluate the accuracy of the identified model, helicopter responses from a flight-data set which was not used for the identification are compared with the responses predicted by the identified model.

4 Application of System Identification

The application of system identification to our small-size unmanned helicopter follows the procedure for full-size helicopters.

Collection of Flight-Data: Flight Experiments

For the collection of flight-data from our experiments, the flight maneuvers were commanded by the pilot via the remote control (RC) unit. To ensure the efficiency of system identification, it is important to conduct the flight experiments open-loop. This was possible for all axes except yaw for which an active yaw damping system was in use. In addition, to help the pilot in controlling the coupled yaw and heave dynamics, the pedal and collective inputs were subject to mixing.

The special flight maneuvers using frequency-sweeps for pilot inputs are the same as those used in full-size helicopters [7]. One separate sweep set is conducted for each of the control inputs. During the time of the experiment, all control inputs (stick inputs) and all helicopter states are recorded with a sampling rate of 100 Hz.

For each experiment, the pilot applies a frequency sweep to the particular control input. While doing so, he uses the remaining three control inputs to maintain the helicopter in trim at the selected operating point (hover flight). In order to gather enough data, the same experiment is repeated four to five times. Flight-data

from the best runs are then concatenated and filtered according to the frequency range of interest (-3 dB @ 10 Hz). A sample flight-data of longitudinal and lateral response for two concatenated lateral frequency sweeps is shown in Figure 2.

The quality of the collected flight-data can be evaluated from the coherence values computed together with the frequency responses. The coherence indicates how well one output is linearly correlated with a particular input over the examined frequency range. A poor coherence can be attributed to either a poor signal to noise ratio or to nonlinear effects in the dynamics. For our flight-data, all on-axis responses attain a coherence close to unity over most of the critical frequency range where the relevant dynamical effects take place. (See Figure 3 in the Appendix.) For example, the two on-axis angular rate responses to the cyclic inputs achieve a good coherence (>0.6) up to the frequencies where the important airframe/rotor coupling takes place. These results speak for the quality of the helicopter instrumentation, the successfully performed flight experiments, and the dominantly linear behavior of the helicopter in hovering flight.

Building the Identification Model Structure

The model structure for our small-size helicopter is largely based on the model structure used for the identification of full-size helicopters. The model structure specifies the order and form of the differential equations which describe the dynamics. Typically, the dynamics of the helicopter are represented as rigid-body (airframe dynamics, 6 degrees of freedom), which can be coupled to additional dynamics such as the rotor or engine/drive-train dynamics. Including these subsystems improves the accuracy of the model for the higher-frequency range and also makes for a model which is physically more consistent (less lumped).

The decision about what to include beyond rigid-body dynamics is made according to the objective of the identification (accuracy/bandwidth of the model) and the actual nature of the dynamics. The nature of the dynamics can be well understood by looking at the frequency responses derived from the flight data. Generally of special interest are the angular (roll and pitch) responses of the helicopter to the cyclic inputs, which constitute the core of the helicopter dynamics.

- Angular dynamics

For our helicopter, the frequency response of the rolling and pitching rates p and q to the lateral and longitudinal cyclic inputs $\delta_{lat}, \delta_{lon}$, (Figure 3 in the Appendix) shows a pronounced underdamped second-order behavior: the magnitude shows a marked, lightly damped resonance followed by a 40dB/dec roll-off, and the phase exhibits a 180° shift. The second order nature of the response is well known in full-size helicopters, and results from the dynamical coupling between the airframe angular motion and the regressive rotor flap dynamics (blade flapping a_{1s}, b_{1s}). The lightly damped characteristic is a function of the setting of the Bell-Hiller stabilizer bar gearing.

The "hybrid model" approach, used in [5,7] is an efficient way to represent the coupled airframe/rotor dynamics. In this modeling approach, the lateral and longitudinal blade flapping dynamics b_{1s}, a_{1s} are described respectively by two coupled first-order differential equations.

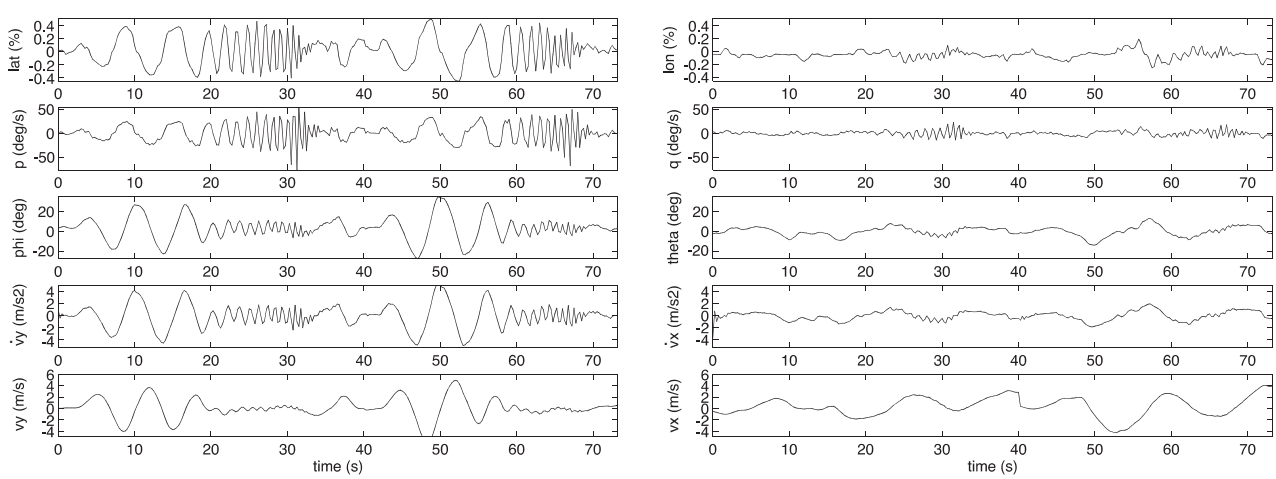

Figure 2 – Sample flight data for two concatenated lateral frequency sweeps

$$\dot{b}_{1s} = -\frac{b_{1s}}{\tau_f} - p + B_{a_{1s}} a_{1s} + B_{lat}\delta_{lat} + B_{lon}\delta_{lon} \quad (1)$$

$$\dot{a}_{1s} = -\frac{a_{1s}}{\tau_f} - q + A_{b_{1s}} b_{1s} + A_{lat}\delta_{lat} + A_{lon}\delta_{lon} \quad (2)$$

In our case, best results were obtained with a coupled lateral-longitudinal flapping rotor dynamics formulation. The rotor time constant τ_f includes the influence of the stabilizer bar.

The rotor itself is coupled to the airframe dynamics through the roll and pitch angular dynamics p, q (Eq. 3-4) and the lateral and longitudinal translational dynamics v and u (Eq. 5-6), through rotor flapping spring terms $L_{b_{1s}}, M_{a_{1s}}, Y_{b_{1s}}, X_{a_{1s}}$.

$$\dot{p} = L_u u + L_v v + L_{b_{1s}} b_{1s} + L_{a_{1s}} a_{1s} \quad (3)$$

$$\dot{q} = M_u u + M_v v + M_{b_{1s}} b_{1s} + M_{a_{1s}} a_{1s} \quad (4)$$

$$\dot{v} = Y_v v + g\phi + Y_{b_{1s}} b_{1s} \quad (5)$$

$$\dot{u} = X_u u - g\theta + X_{a_{1s}} a_{1s} \quad (6)$$

Good results were obtained using the hybrid model structure; however, the results were further improved by the addition of the off-axis spring terms: $M_{b_{1s}}, L_{a_{1s}}$. Since the cross-axis effects are being accounted for in the rotor equations (Eq. 1-2) the additional cross-axis effects are apparently related to a noticeable tilt of the hub/shaft system relative to the fuselage axes.

The derivatives $Y_{b_{1s}}, X_{a_{1s}}$ should theoretically be equal respectively to plus and minus the value of the gravity ($g = 32.2\, ft/s^2$). Constraining the two derivatives, however, can only be enforced if the flight data has been accurately corrected for an offset in the measurement system location relative to the c.g.. Since, in our case, the c.g. location is not known with sufficient accuracy, we have explicitly accounted for a vertical offset h_{cg} by relating the measured speeds (v_m, u_m) to the speed at the c.g. (v, u).

$$v_m = v - h_{cg} p \quad (7)$$

$$u_m = u + h_{cg} q \quad (8)$$

Using this method we were able to enforce the constraint $-X_{a_{1s}} = Y_{b_{1s}} = g$ and at the same time identify the unknown vertical offset h_{cg}.

- Heave dynamics

With regard to the heave dynamics, after examination of the respective frequency response (Figure 3, VZdot/COL in the Appendix), we see that a first order system should adequately capture the dynamics. The corresponding differential equation is:

$$\dot{z} = Z_w w + Z_{col}\delta_{col} \quad (9)$$

Note that the response does not exhibit the peak in magnitude caused by the inflow dynamics, a peak which is typical in full-size helicopters. This is because the flap frequency for the R-50 (1/rev=89 rad/sec) is well beyond the frequency range of identification and of piloted excitation (30 rad/sec).

- Yaw dynamics

Because of the use of an artificial yaw-damping system during the flight experiments, the yaw response exhibits a second order nature. To allow for an accurate identification, the model structure must account for this system.

The bare airframe yaw dynamics can be modeled as a first order system with transfer function:

$$\frac{r}{\delta_{ped}} = \frac{N_{ped}}{s - N_r} \quad (10)$$

The artificial yaw damping is achieved using a yaw rate feedback r_{fb}; we assume that the yaw rate feedback can be modeled as a simple first order low-pass filter with transfer function:

$$\frac{r_{fb}}{r} = \frac{K_r}{s + K_{rfb}} \quad (11)$$

Closing the loop leads to the following transfer function for the response between the pilot input δ_{ped} and the yaw r:

$$\frac{r}{\delta_{ped}} = \frac{N_{ped}(s + K_{rfb})}{s^2 + (K_{rfb} - N_r)s + (K_r N_{ped} - N_r K_{rfb})} \quad (12)$$

The equivalent differential equations used for the state-space model are:

$$\dot{r} = N_r r + N_{ped}(\delta_{ped} - r_{fb}) \quad (13)$$

$$\dot{r}_{fb} = -K_{rfb} r_{fb} + K_r r \quad (14)$$

Since we have only the measurements of the pilot input δ_{ped} and the yaw rate r, this representation is over-parameterized. One constraint between two parameters must be added to enable successful identification of the parameters. As constraint, we have stipulated that the pole of the low-pass filter must be twice as fast as the pole of the bare airframe yaw dynamics, i.e.,:

$$K_{rfb} = -2 \cdot N_r \quad (15)$$

With this constraint, a low transfer function cost was attained, and the resulting parameters are physically meaningful, i.e., a good estimate of the bare airframe yaw damping N_r can be achieved.

Full Model Structure

The complete model structure is obtained by collecting all the differential equations in the matrix differential

equation:

$$\dot{\bar{x}} = F\bar{x} + G\bar{u} \tag{16}$$

with state vector:

$$\bar{x} = \begin{bmatrix} u & v & p & q & \phi & \theta & a_{1s} & b_{1s} & w & r & r_{fb} \end{bmatrix}^T \tag{17}$$

and input vector:

$$\bar{u} = \begin{bmatrix} \delta_{lat} & \delta_{lon} & \delta_{ped} & \delta_{col} \end{bmatrix}^T \tag{18}$$

The different states are further coupled according to the coherence obtained in the respective cross axis frequency responses. For example, the heave dynamics couples with the yaw dynamics through the derivatives Z_r and N_w, N_{col}. The heave dynamics is also influenced by the rotor flapping through the derivatives $Z_{a_{1s}}, Z_{b_{1s}}$.

The final structure is obtained by first systematically eliminating the derivatives that have high insensitivity and/or are highly correlated, and then reconverging the model in a process described in [5]. The remaining minimally parameterized model structure is given by the system matrix F and the input matrix G, shown in Table 2.

5 Results

The converged model exhibits an excellent fit of the frequency response data and an associated outstanding overall frequency-response error cost of 45 (Table 3), which is about half the best values obtained in full scale identification results. Table 6 in the Appendix gives the numerical values of the identified derivatives and their associated accuracy statistics: the Cramer Rao bound (%) and the insensitivity (%) of the derivatives. These statistics indicate that all of the key control and response parameters are extracted with a high degree of precision [5]. Notice that most of the quasi-steady derivatives have been dropped, thus showing that the rotor plays a dominant role in the dynamics of small-size helicopters. This is also reflected by the number of rotor flapping derivatives $(\ )_{b1s}$ or $(\ )_{a1s}$. The term "actuated" helicopter is a good idealization of the dynamics of the small-size helicopter, where the actuator, i.e., the rotor, dominates the response.

An important result is the identified large rotor flap time constant $\tau_f = 0.38\,\text{sec} \approx 5.4\ rev$, which is due to the stabilizer bar as discussed earlier. The identified rotor angular-spring derivatives and quasi-steady damping derivatives (e.g., $L_{b1s}, M_{a1s}, X_u, Y_v, Z_w, N_r$) have the sign and *relative* magnitudes expected for hovering helicopters, but the absolute magnitudes are all considerably larger (2-5 times) than those for full scale aircraft. This is expected from the dynamic scaling relationships as discussed later herein.

With the help of the offset equations (Eq. 7-8) we were able to constrain the force coupling derivatives to gravity $(-X_{a_{1s}} = Y_{b_{1s}} = g)$ and, at the same time, identify the vertical c.g. offset which came out to be $h_{cg} = -0.5\ ft$.

The lateral and longitudinal speed derivatives (M_u, L_v) contribute a destabilizing influence on the phugoid dynamics.

Finally, the time delays, which account for higher-order rotor and inflow dynamics, processing, and filtering effects, are small and accurately determined. This indicates that the hybrid model structure accurately captures the key dynamics.

Eigenvalues and Modes of Motion

The key dynamics of the R-50 are clearly seen from reference to the system's eigenvalues and eigenvectors

(see Table 4). The first four roots (eigenvalues #1-4) are essentially on the real axis, two roots being stable and two unstable. The unstable modes (eigenvalues #1-

$$F = \begin{bmatrix}
X_u & 0 & 0 & 0 & 0 & -g & X_{a_{1s}} & 0 & 0 & 0 & 0 \\
0 & Y_v & 0 & 0 & g & 0 & 0 & Y_{b_{1s}} & 0 & 0 & 0 \\
L_u & L_v & 0 & 0 & 0 & 0 & L_{a_{1s}} & L_{b_{1s}} & 0 & 0 & 0 \\
M_u & M_v & 0 & 0 & 0 & 0 & M_{a_{1s}} & M_{b_{1s}} & 0 & 0 & 0 \\
0 & 0 & 1 & 0 & 0 & 0 & 0 & 0 & 0 & 0 & 0 \\
0 & 0 & 0 & 1 & 0 & 0 & 0 & 0 & 0 & 0 & 0 \\
0 & 0 & 0 & -1 & 0 & 0 & -1/\tau_f & 0 & 0 & 0 & 0 \\
0 & 0 & -1 & 0 & 0 & 0 & B_{a_{1s}} & -1/\tau_f & 0 & 0 & 0 \\
0 & 0 & 0 & 0 & 0 & 0 & Z_{a_{1s}} & Z_{b_{1s}} & Z_w & Z_r & 0 \\
0 & 0 & N_p & 0 & 0 & 0 & 0 & 0 & N_w & N_r & MN_{ped} \\
0 & 0 & 0 & 0 & 0 & 0 & 0 & 0 & 0 & K_r & MK_{rfb}
\end{bmatrix}
\quad
G = \begin{bmatrix}
0 & 0 & 0 & 0 \\
0 & 0 & 0 & 0 \\
0 & 0 & 0 & 0 \\
0 & 0 & 0 & 0 \\
0 & 0 & 0 & 0 \\
0 & 0 & 0 & 0 \\
A_{lat} & A_{lon} & 0 & 0 \\
B_{lat} & B_{lon} & 0 & 0 \\
0 & 0 & 0 & Z_{col} \\
0 & 0 & N_{ped} & N_{col} \\
0 & 0 & 0 & 0
\end{bmatrix}$$

Table 2 - System and input matrix for the state-state model

Transfer Function	Cost
VX /LAT	24.884
VY /LAT	21.941
P /LAT	59.462
Q /LAT	99.511
AX /LAT	24.884
AY /LAT	27.927
R /LAT	43.006
AZ /LAT	47.469
VX /LON	38.731
VY /LON	47.747
P /LON	101.110
Q /LON	67.118
AX /LON	38.731
AY /LON	47.747
AZ /LON	25.681
R /COL	42.241
AZ /COL	21.673
R /PED	63.530
AZ /PED	9.875
Average	44.909

Table 3 - Transfer function costs

2) involve the horizontal velocities with both attitude angles. The stable modes (eigenvalues #3-4) involve the horizontal and vertical velocities.

The damped real mode (eigenvalue #5) is associated with the heave response The well damped oscillatory pair (eigenvalues #6-7) is the closed-loop yawing mode resulting from the active yaw damping system.

In the high-frequency range, the two very lightly damped modes correspond to the coupled fuselage/flapping/stabilizer-bar modes. First, the pitching mode (eigenvalues #8-9), which has a considerable roll coupling component (50%), has a frequency that is nearly exactly the square root of the pitch flap spring ($\sqrt{M_{a1s}} = 8.2 \text{rad/sec}$). Similarly, the coupled rolling mode with slight pitching component (10%) (eigenvalues #10-11), has a frequency that corresponds to the square root of the roll flap spring ($\sqrt{L_{b1s}} = 11.9 \text{rad/sec}$). The small damping ratio directly reflects the large rotor time constant. For example in the roll axis:

$$\zeta_{roll-flap} = 1/(2\tau_f \sqrt{L_{b1s}}) = 0.11, \qquad (17)$$

which agrees with the complete system eigenvalue result. This damping ratio for the coupled fuselage/flapping/stabilizer-bar dynamics is typical for full scale helicopters employing a stabilizer bar [4]. The strongly-coupled fuselage/flapping modes emphasize once more the importance of the rotor dynamics.

λ# mode type	Re(λ)	Im(λ)	ζ	ω (r/s)
1-2 phugoid 1	0.287 0.287	0.064 -0.064	-0.976 -0.976	0.294 0.294
3-4 phugoid 2	-0.454 -0.454	0.046 -0.046	0.995 0.995	0.457 0.457
5 heave	-0.495	0	0	0
6-7 yaw-heave	-4.12 -4.12	5.97 -5.97	0.567 0.567	7.26 7.26
8-9 pitch	-1.25 -1.25	8.28 -8.28	0.149 0.149	8.37 8.37
10-11 roll	-1.41 -1.41	-11.8 11.8	0.119 0.119	11.85 11.85

Table 4 - Eigenvalues and modes for hover

Dynamic Scaling

A further understanding of the small-scale R-50 identification results is achieved through a comparison with the characteristics of a conventional teetering rotor configuration (UH-1H), dynamically scaled to the same rotor diameter. Dynamic (or "Froude") scaling ensures that the model scale and full scale vehicles share common ratios of inertia-to-gravity forces, and aero-to-gravity forces. The geometric and dynamic characteristics of the model scale (m) and full scale aircraft (a) are then related via a well known standard set of similarity laws [8] based on scale ratio N (e.g., N=5 refers to a 1/5th scale model):

Length:	$L_m = L_a / N$
Time constant:	$T_m = T_a / \sqrt{N}$
Weight:	$W_m = W_a / N^3$
Moment of inertia:	$I_m = I_a / N^5$
Frequency:	$\omega_m = \omega_a \sqrt{N}$

Table 5 compares the key configuration parameters and identified dynamic characteristics for the R-50 with the model-scale equivalents for the UH-1H. The scale ratio is N=4.76, or nearly 1/5th scale. The R-50 is seen to be about twice as heavy as a scaled down UH-1H, due to the payload weight (53lbs.), which results in a higher normalized thrust coefficient (C_T/σ) than would otherwise be expected. The R-50 blades are also relatively heavier, giving a lower Lock number than the UH-1H. These increased relative weights appear to be typical of small-scale flight vehicles as seen from reference to the scaled data for the TH-55 [9]. The higher flap spring is due to the elastomeric teetering restraint on the R-50, and is equivalent to an effective hinge-offset of about 3%. The resulting roll/flap

Parameter	R-50	scaling	UH-1H full-scale	UH-1H model-scale
R, Rotor rad.(ft)	5.04	1/N	24	5.04
W, Weight (lb)	150	$1/N^3$	8000	74
Ω, Rotor rotation rate (r/s)	89.01	$\sqrt{N}$	34	76.1
I_β ,Blade inertia,(s-ft^2)	0.87	$1/N^5$	1211	0.495
γ, Lock number	3.44	1	6.5	6.5
C_T/σ	0.0896	1	0.0606	0.0606
h_{rot}/R , rotor hub height	0.36	1	0.29	0.29
L_{b1s}, flap spring (r/s^2)	142.5	N	19.2	96.77
ω_{rf} roll/flap freq,(r/s)	11.85	$\sqrt{N}$	4.38	9.83
$\tau_f\Omega$, non-dim. rotor flap time constant (rotor rev.)	5.4	1	5.7	5.7

Table 5 – Comparison of R-50 and dynamically-scaled UH-1H characteristics, N=4.76

frequency is 20% higher than the scaled equivalent UH-1H. Finally, the non-dimensional rotor time constants are essentially identical (about 5 revs), showing the same strong effect of the stabilizer bar on both aircraft. Despite some detailed differences, the R-50 is seen to be dynamically quite similar to the UH-1H.

Frequency Response Comparisons

The frequency responses from the identified model match the flight data well as seen in Figure 3 in the Appendix. This matching is expected from the very low cost functions of Table 3. The poorest match is obtained for the angular dynamics' cross axis responses (p to δ_{lon} and q to δ_{lat}). If we look at the corresponding diagram in Figure 3, we can see that the corresponding responses exhibit a phase mismatch. Better results could be achieved if the stabilizer bar were modeled explicitly instead of lumping its dynamics into the rotor equations (Eq. 1-2).

Once again, this close agreement is somewhat better than what is usually achieved in full-size helicopters. This can be attributed to the dynamics of the small-size helicopter being dominated by the rotor dynamics and the absence of complex aerodynamic effects.

Time Domain Verification

Time domain verification was conducted by driving the identified models with flight data not used in the identification process. The results, which are presented in Figure 4 and 5 in the Appendix, show an excellent agreement between the model predictions and the flight data for all control axes and outputs except the yaw response, where a small amount of mismatch is present. This is accounted for by the presence of the active yaw damping system and the mixing between the pedal and collective input. Better results could be obtained if both systems were disabled during the flight experiments or if the actual actuator inputs were measured.

6 Conclusion

1. System identification techniques as used in full-size helicopters can be successfully applied to small-size unmanned helicopters. Small-size helicopters seem to be particularly well suited to identification. This is partly due to the dominance of the rotor in the dynamics and the absence of complex aerodynamic and structural dynamic effects.
2. Good results were made possible because of the state of the art instrumentation system, including: IMU, GPS, and Kalman filter.
3. CIFER® system identification techniques were effectively used to derive an accurate high-bandwidth model for the hovering helicopter (for the conditions present during the flight-data collection.) The identified model is well suited to flight control and simulation applications.
4. The R-50 was shown to be dynamically quite similar to the scaled UH-1H. However, the R-50 is proportionally heavier (aircraft weight and blade inertia) and has a small effective hinge-offset (3%) due to the elastomeric teetering restraint. The dynamics of both helicopters are strongly influenced by the stabilizer bar.

Outlook

Currently, a next generation Yamaha helicopter ("R-MAX") is being instrumented at Carnegie Mellon. The new system will allow access to the position of the individual actuators and, in addition, a blade flapping measurement system is being developed. With this system, comprehensive identification studies and potentially rotor state feedback will be possible. The flight experiments and model identification will all be extended to forward flight and, in parallel, we will start using the derived models for flight control design.

Acknowledgements

This work is made possible thanks to the collaboration of Omead Amidi, Mark DeLouis, Ryan Miller and Chuck Thorpe, and the support of Yamaha Motor Corporation and funding under NASA Grant NAG 2-1276.

References

[1] "Operational Requirements Document for the Vertical Takeoff and Landing Tactical Unmanned Aerial Vehicle *(VTUAV)* " US Navy.

[2] Tischler, M.B., "System identification requirements for high-bandwidth rotorcraft flight control system design. " *Journal of Guidance and Control*, 1990. **13(5)**: p. 835-841.

[3] Amidi, O., T. Kanade, and R. Miller. "Autonomous Helicopter Research at Carnegie Mellon Robotics Institute." *Proceedings of Heli Japan '98*. 1998. Gifu, Japan.

[4] Heffley, R. K., Jewell, Lehmam J. M., Von Winkle, R. A, "A Compilation and Analysis of Helicopter Handling Qualities Data; Volume I: Data Compilation." NASA CR 3144, August, 1979.

[5] Tischler, M.B. and M.G. Cauffman, "Frequency-Response Method for Rotorcraft System Identification: Flight Application to BO-105 Coupled Rotor/Fuselage Dynamics." *Journal of the American Helicopter Society*, 1992. **37/3**: p. 3-17.

[6] Tischler, M. B., "System Identification Methods for Aircraft Flight Control Development and Validation." *Advances in Aircraft Flight Control*. Taylor & Francis, 1996.

[7] Ham, J.A., C.K. Gardner, and M.B. Tischler, "Flight-Testing and Frequency-Domain Analysis for Rotorcraft Handling Qualities." *Journal of the American Helicopter Society*, 1995(April 1995).

[8] Burk, S. M., Wilson, C. F, Jr., "Radio-Controlled Model Design and Testing Techniques for Stall/Spin Evaluation of General-Aviation Aircraft." SAE National Business Aircraft Meeting, 1975.

[9] Heffley, R. K, et al, "Study of Helicopter Roll Control Effectiveness Criteria." NASA CR177404, April, 1986.

Appendix

A1. Table of Identified Derivatives

Derivative	Identified Value	Cramer Rao Bound (%)	Insens. (%)
F-Matrix			
TF	0.3753	4.359	0.5814
HCG	-0.4958	4.392	1.564
MHCG	0.4958	constrained (= -HCG)	
XU	-0.09865	32.68	16.01
XTHE	-32.2	constant (= -g)	
XA1S	-32.2	constant (= -g)	
YV	-0.2289	15.65	7.649
YPHI	32.2	constant (= g)	
YB1S	32.2	constant (= g)	
LU	-0.2111	12.00	2.524
LV	0.1505	20.58	7.902
LB1S	142.5	1.378	0.4812
LA1S	22.14	6.168	1.536
MU	-0.08550	15.32	3.183
MV	-0.05298	16.50	5.618
MB1S	-7.366	16.59	6.509
MA1S	67.74	1.618	0.4946
BA1S	0.5543	7.191	1.677
ZB1S	-121.2	4.664	1.489
ZA1S	-28.85	8.239	2.439
ZW	-0.5024	11.42	4.897
ZR	0.9418	8.309	2.757
NP	-3.126	8.149	2.923
NW	0.07237	12.90	4.475
NR	-2.742	10.26	2.441
MNPED	-21.74	constrained (= -NPED)	
KR	1.731	6.595	1.767
MKRFB	5.483	constrained (= 2 NR)	
G-Matrix			
BLAT	0.4448	5.057	0.9598
BLON	0.03773	9.837	3.031
ALAT	0.05685	7.071	1.963
ALON	-0.3824	4.917	0.7808
ZCOL	40.23	4.191	1.820
NCOL	2.303	10.37	3.744
NPED	21.74	5.376	1.531
TPED	0.1001	5.384	2.552
TCOL	0.04987	11.26	5.576

Table 6 - Identified derivatives and associated accuracy statistics

A2. Frequency Response Results

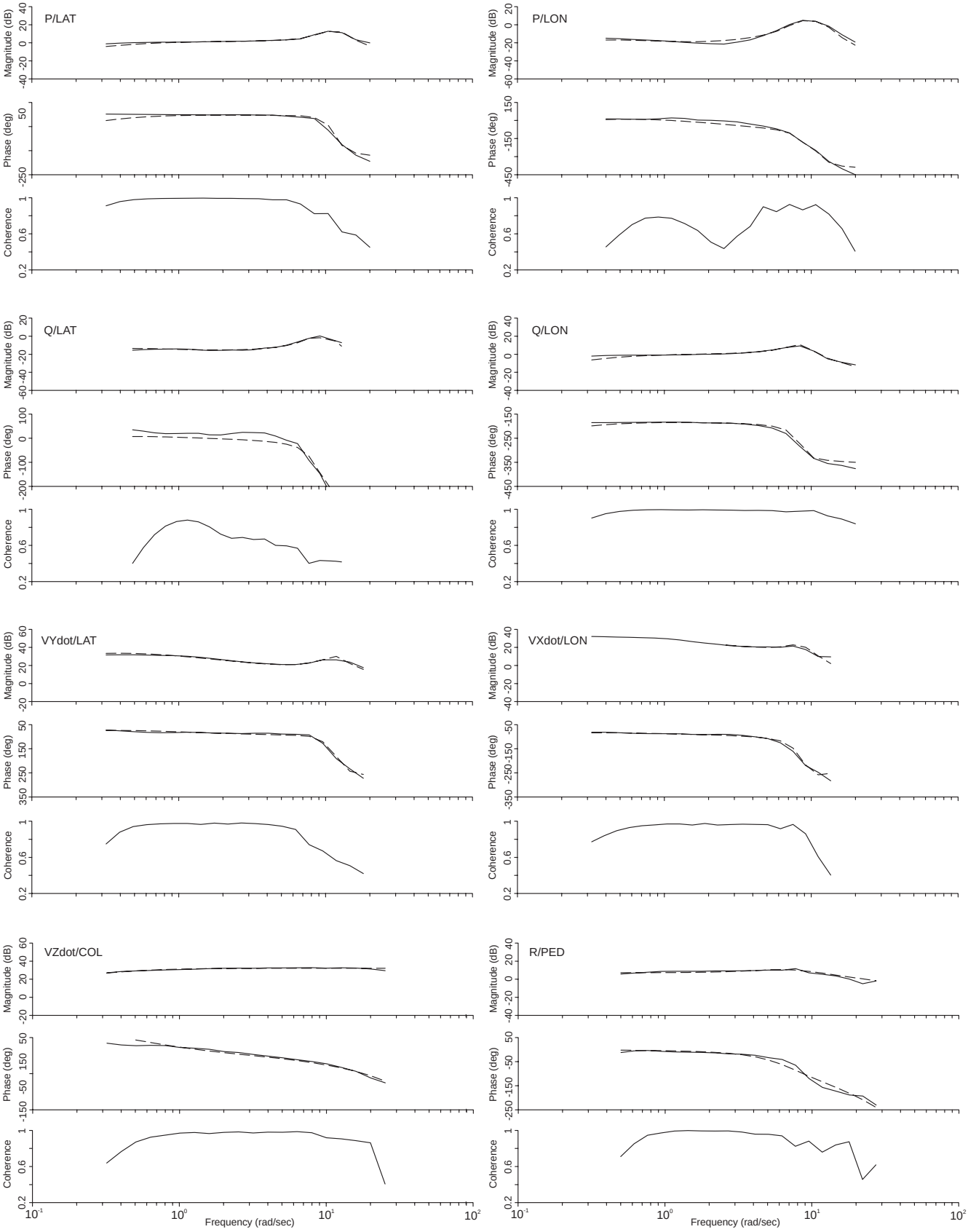

Figure 3 - Frequency response comparisons of identified model (dashed line) with flight data (solid line)

A3 Time Domain Verification Results

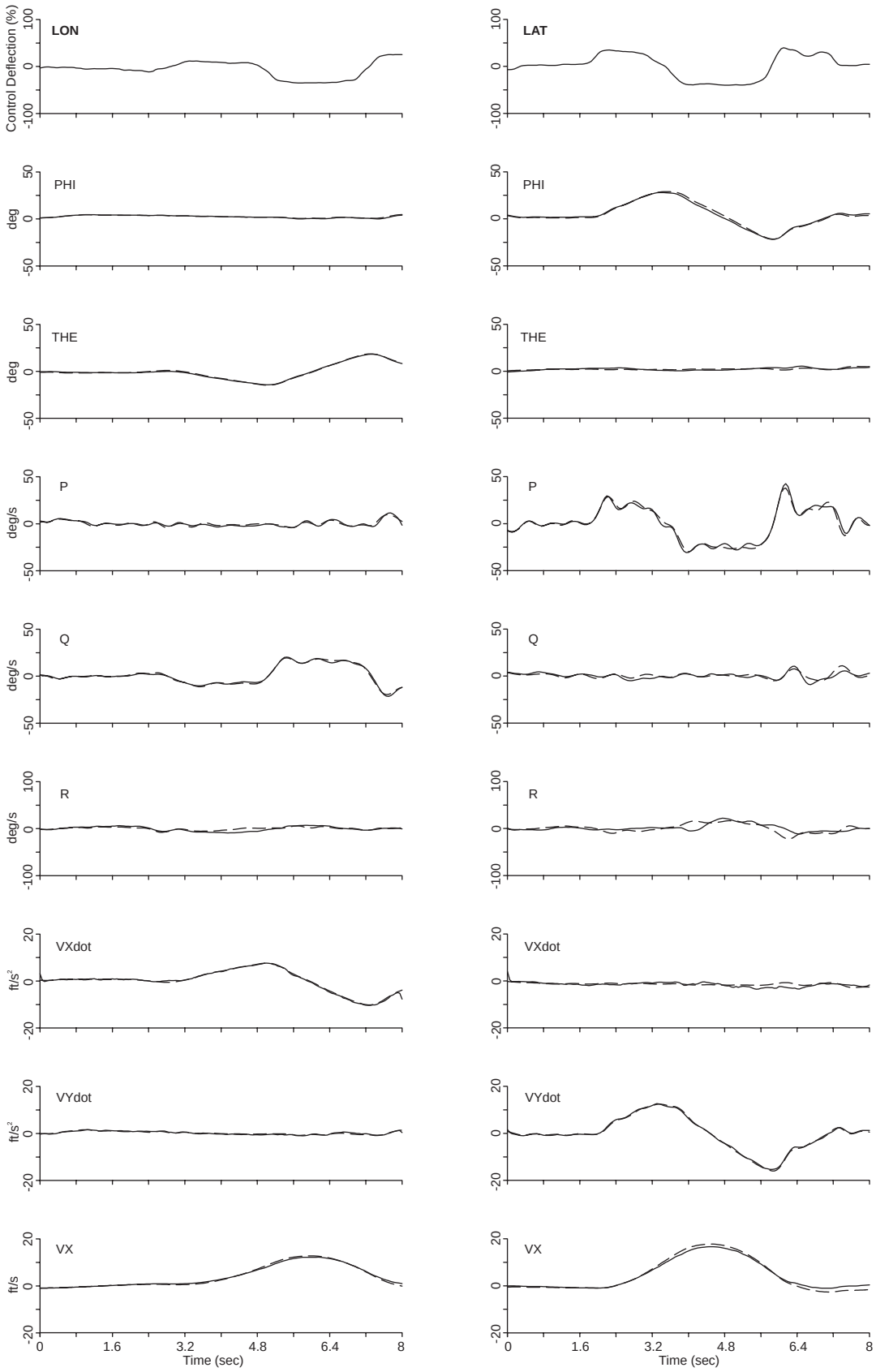

Figure 4 - Time domain verification of identified model responses (dashed line) for longitudinal and lateral inputs

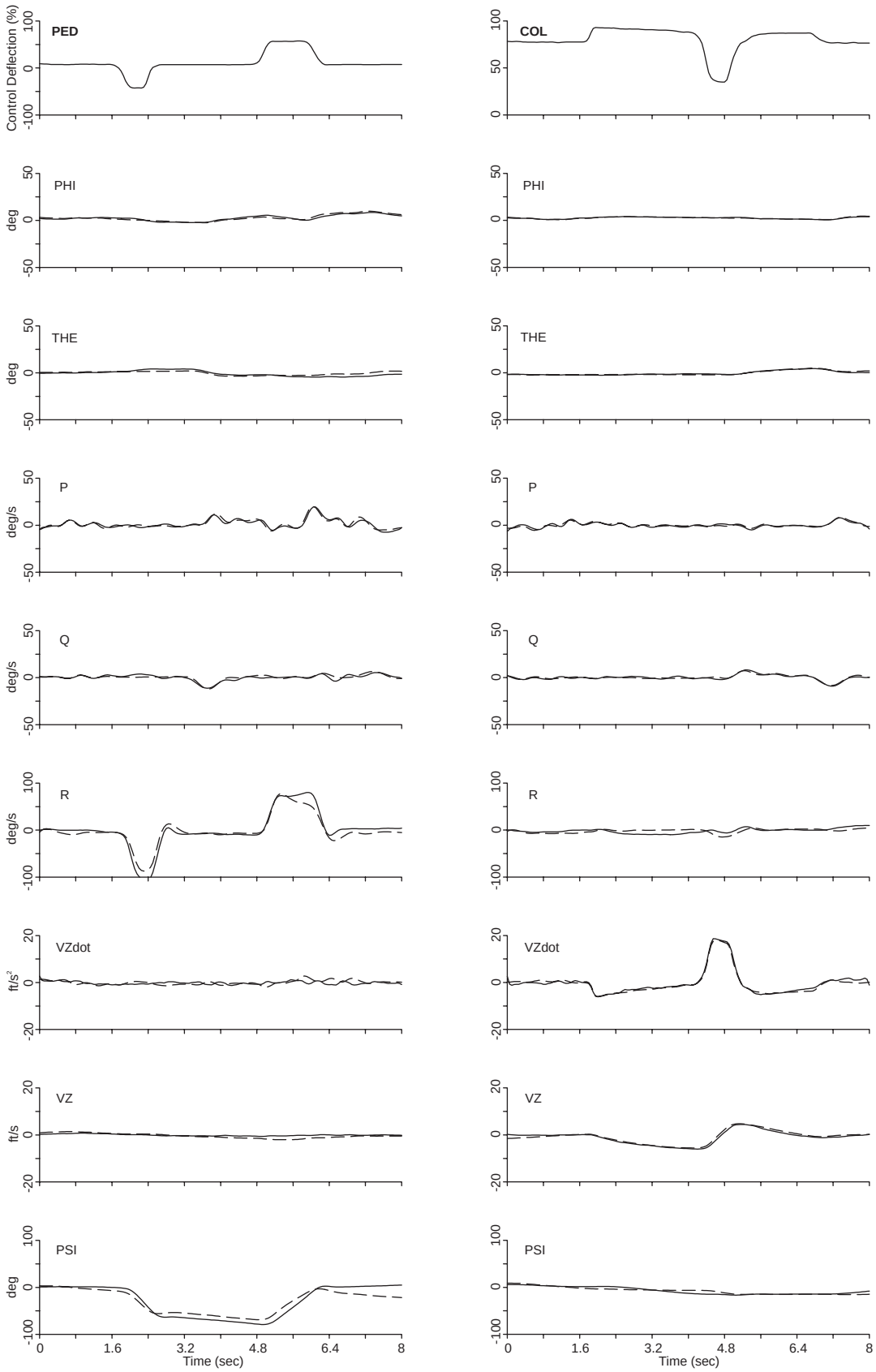

Figure 5 - Time domain verification of identified model responses (dashed line) for pedal and collective inputs